

Article

Association Behavior of Amphiphilic ABA Triblock Copolymer Composed of Poly(2-methoxyethyl acrylate) (A) and Poly(ethylene oxide) (B) in Aqueous Solution

Yoko Mizoue ¹, Ema Onodera ¹, Kazutoshi Haraguchi ² and Shin-ichi Yusa ^{1,*} 

¹ Department of Applied Chemistry, Graduate School of Engineering, University of Hyogo, 2167 Shosha, Himeji 671-2280, Hyogo, Japan; ym85725@gmail.com (Y.M.); e629ma.o@gmail.com (E.O.)

² Department of Applied Molecular Chemistry, College of Industrial Technology, Nihon University, 1-2-1 Izumicho, Narashino 275-8575, Chiba, Japan; haraguchi.kazutoshi@nihon-u.ac.jp

* Correspondence: yusa@eng.u-hyogo.ac.jp; Tel.: +81-79-267-4954; Fax: +81-79-266-8868

Abstract: Poly(2-methoxyethyl acrylate) (PMEA) and poly(ethylene oxide) (PEO) have protein-antifouling properties and blood compatibility. ABA triblock copolymers (PMEA_l-PEO₁₁₃₄₀-PMEA_m (MEOM_n; *n* is average value of *l* and *m*)) were prepared using single-electron transfer-living radical polymerization (SET-LRP) using a bifunctional PEO macroinitiator. Two types of MEOM_n composed of PMEA blocks with degrees of polymerization (DP = *n*) of 85 and 777 were prepared using the same PEO macroinitiator. MEOM_n formed flower micelles with a hydrophobic PMEA (A) core and hydrophilic PEO (B) loop shells in diluted water with a similar appearance to petals. The hydrodynamic radii of MEOM₈₅ and MEOM₇₇₇ were 151 and 108 nm, respectively. The PMEA block with a large DP formed a tightly packed core. The aggregation number (*N*_{agg}) of the PMEA block in a single flower micelle for MEOM₈₅ and MEOM₇₇₇ was 156 and 164, respectively, which were estimated using a light scattering technique. The critical micelle concentrations (CMCs) for MEOM₈₅ and MEOM₇₇₇ were 0.01 and 0.002 g/L, respectively, as determined by the light scattering intensity and fluorescence probe techniques. The size, *N*_{agg}, and CMC for MEOM₈₅ and MEOM₇₇₇ were almost the same independent of hydrophobic DP of the PMEA block.

Keywords: flower-like micelle; triblock copolymer; amphiphilic copolymer; single-electron transfer-living radical polymerization; poly(ethylene oxide)



Citation: Mizoue, Y.; Onodera, E.; Haraguchi, K.; Yusa, S.-i. Association Behavior of Amphiphilic ABA Triblock Copolymer Composed of Poly(2-methoxyethyl acrylate) (A) and Poly(ethylene oxide) (B) in Aqueous Solution. *Polymers* **2022**, *14*, 1678. <https://doi.org/10.3390/polym14091678>

Academic Editor: Ian Wyman

Received: 17 March 2022

Accepted: 18 April 2022

Published: 20 April 2022

Publisher's Note: MDPI stays neutral with regard to jurisdictional claims in published maps and institutional affiliations.



Copyright: © 2022 by the authors. Licensee MDPI, Basel, Switzerland. This article is an open access article distributed under the terms and conditions of the Creative Commons Attribution (CC BY) license (<https://creativecommons.org/licenses/by/4.0/>).

1. Introduction

Amphipathic block copolymers form interpolymer aggregates because of the hydrophobic interactions of hydrophobic blocks in water [1]. Generally, amphipathic AB diblock copolymers form core-shell spherical polymer micelles in water. ABA triblock copolymers with two hydrophobic A blocks at both ends of the central B block form flower-like micelles caused by interpolymer aggregation in water [2]. The hydrophobic A blocks aggregate to form a core, and the hydrophilic B blocks form loop shape shells with a similar appearance to petals on the surface of the core to form flower micelles. The flower micelles are bridged when the hydrophobic A blocks in the ABA triblock copolymer are incorporated into separate cores in flower micelles. With increasing polymer concentration (*C*_p), the number of bridges between the flower micelles increases to form a gel [3]. The polymers increase the viscosity of the aqueous solution to form interpolymer aggregates, which can then be applied as associative thickeners with a small amount of addition [4]. For example, flower micelles formed from ABA triblock copolymers have been applied as associative thickeners [5]. Associative thickeners are used in water-based paints, coatings, personal care goods, and adhesive agents [6].

The hydrophilic shells on the surface of polymer micelles formed from amphipathic block copolymers stabilize the micelle structure and maintain their dispersion stability in

solution [7]. Polymer micelles formed from high molecular weight polymers generally have a lower critical micelle concentration (CMC) and higher colloidal stability than those formed from low molecular weight surfactants [8]. The CMC of amphiphilic diblock copolymers depends on the ratio of the hydrophobic to hydrophilic block lengths. CMC decreases with increasing hydrophobic block chain length for a constant hydrophilic block chain length in the diblock copolymer [9–11]. Zhulina et al. [12] studied thermodynamic properties of block copolymer micelles. With ABA triblock copolymers, the CMC also decreases with increasing hydrophobic block chain length [13]. Borisov and Halperin reported theoretical models of flower micelles [14].

Single-electron transfer-living radical polymerization (SET-LRP) is a method for controlled radical polymerization using a copper catalyst [15]. A copper catalyst is widely used as an inorganic electron donor reagent for organic and polymer syntheses (Figure S1). SET-LRP can be performed at low temperatures, e.g., room temperature, because of the low activation energy [16]. Poly(ethylene oxide) (PEO) is often used as a hydrophilic block in amphiphilic ABA triblock copolymers because it can form flower micelles easily [17,18]. Furthermore, PEO is widely used in biomedical and biomaterial fields owing to its biocompatibility [19]; 2-Methoxyethyl acrylate (MEA) is an acrylate monomer that can be polymerized by radical polymerization [20]. Poly(2-methoxyethyl acrylate) (PMEA) is highly blood compatible because it has a protein-antifouling effect, and platelets cannot adhere easily to PMEA [21,22]. PMEA forms an intermediate water layer on its surface to suppress protein adsorption [23]. Furthermore, PMEA can be applied as coatings on various substrates because PMEA can be soluble in organic solvents, water insoluble, transparent, and adhesive [24]. Owing to the excellent properties of PMEA, it is also used as a coating material for artificial organs [25]. Haraguchi et al. [26,27] reported protein antifouling and blood compatible coatings using amphiphilic ABA triblock copolymers composed of hydrophobic PMEA (A) and hydrophilic poly(*N,N*-dimethylacrylamide) (B). The hydrophobic PMEA (A) blocks show good adhesion to both organic and inorganic substrates.

In this study, ABA triblock copolymers (PMEA_{*l*}-PEO₁₁₃₄₀-PMEA_{*m*} (MEOM_{*n*}; *n* is average value of *l* and *m*)) were prepared by SET-LRP to polymerize MEA using a bifunctional PEO macroinitiator at both chain ends. In particular, we are interested in the association behavior of ABA triblock copolymers with long PEO (B) block in water. MEOM_{*n*} was composed of a hydrophobic PMEA (A) block and a hydrophilic PEO (B) block. In water, MEOM_{*n*} formed flower micelles with a hydrophobic PMEA core and PEO loop-shaped shells (Figure 1). The associative behavior of the flower micelles formed from MEOM_{*n*} in dilute aqueous solutions was examined using dynamic light scattering (DLS), static light scattering (SLS), transmission electron microscopy (TEM), and fluorescence probe technique.

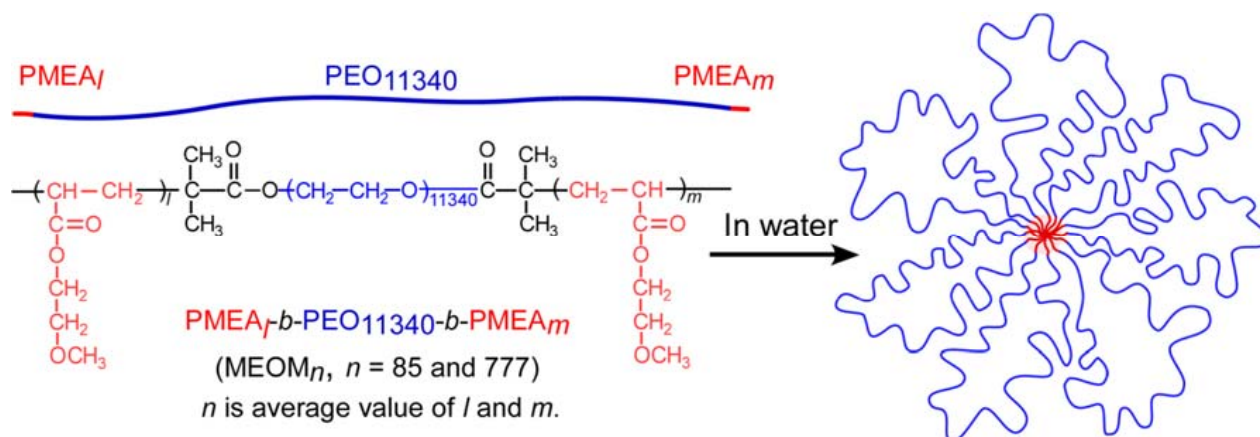


Figure 1. Conceptual illustration of flower micelles formed from MEOM_{*n*} (*n* = 85 and 777).

2. Materials and Methods

2.1. General

Tris(2-(dimethylamino)ethyl)amine (Me₆TREN, 97%) was obtained from Sigma-Aldrich (St. Louis, MO, USA). Copper bromide (CuBr, 95.0%) was supplied by Kishida Chemical (Osaka, Japan). Ethanol (99.5%), tetrahydrofuran (THF, 99.5%), and cetylpyridinium chloride (90%) were purchased from Fujifilm Wako Pure Chemical (Osaka, Japan). All chemicals were used as received; 2-Methoxyethyl acrylate (MEA, 98.0%) from Fujifilm Wako Pure Chemical (Osaka, Japan) was treated with an inhibitor-remover prepacked column from Sigma-Aldrich (St. Louis, MO, USA) prior to use. PEO (MW = 500,000 g/mol) was purchased from Fujifilm Wako Pure Chemical (Osaka, Japan). PEO-based macroinitiator (PEO-Br) was prepared and purified in accordance with the literature [28]. Number average molecular weight (M_n (GPC)) and molecular weight distribution (M_w/M_n) estimated from gel-permeation chromatography (GPC) for PEO-Br were 4.64×10^5 g/mol and 1.23, respectively. The degree of polymerization (DP) for PEO-Br was 11,340. Pyrene (97%) from Fujifilm Wako Pure Chemical (Osaka, Japan) was recrystallized from methanol. Water was purified using an ion-exchange column system.

2.2. Preparation of MEOM_n ($n = 85$ and 777)

MEOM₈₅ was prepared via SET-LRP (Scheme S1). Me₆TREN (2.13 mg, 3.01 μ mol) was dissolved in water (1.00 mL) and stirred under an argon atmosphere for 10 min. CuBr (2.96 mg, 20.6 μ mol) was then added, and the mixture was stirred for 10 min. PEO-Br (M_n (GPC) = 4.64×10^5 g/mol, 1.50 g, 3.01 μ mol) and MEA (420 mg, 3.22 mmol) were dissolved in water (21.3 mL). The aqueous CuBr/Me₆TREN solution was added to an aqueous PEO-Br and MEA solution under an argon atmosphere. The reaction solution was stirred for 71 h under an argon atmosphere at room temperature. The conversion of MEA was 16.8%, which was estimated by ¹H nuclear magnetic resonance (NMR) spectroscopy before purification. The polymerization mixture was dialyzed against pure water for three days, and the polymer (MEOM₈₅) was collected by freeze-drying (0.889 g, 46.3%). The DP of the PME block was 85, as estimated from the ¹H NMR spectrum. The M_n (GPC) and M_w/M_n estimated from GPC were 5.41×10^5 g/mol and 1.17, respectively.

MEOM₇₇₇ was prepared using the same procedure (2.42 g, 63.7%). The conversion of MEA before purification was 34.9%, according to ¹H NMR spectroscopy. The DP of the PME block was 777, as estimated from the ¹H NMR spectrum. The M_n (GPC) and M_w/M_n were 4.91×10^5 g/mol and 1.26, respectively.

2.3. Preparation of MEOM₇₇₇ Aqueous Solution

MEOM₇₇₇ (5.86 mg, 8.35 μ mol) was dissolved in THF (6.02 mL), and the C_p was adjusted to 1.00 g/L. The THF solution was dialyzed against pure water for two days to remove THF. After dialysis, the aqueous solution was diluted with water to be $C_p = 0.10$ g/L.

2.4. Measurements

Using a Bruker (Billerica, MA, USA) DRX-500 and JEOL (Tokyo, Japan) JNM-ECZ400R at 25 °C, ¹H NMR spectroscopy was performed. The water suppression by gradient-tailored excitation (Watergate) with a double pulse field gradient spin echo pulse sequence was used for the D₂O solutions to suppress the water signal. Water suppression by a gradient-tailored excitation (WATERGATE) method was used for the D₂O sample to reduce the water signal. The GPC measurements were conducted at 40 °C using a Shodex (Tokyo, Japan) DS-4 pump, a Shodex GF-7M column, and a Shodex RI-101 refractive index detector. THF was used as the eluent with a flow rate of 1.0 mL/min. M_n (GPC) and M_w/M_n were determined using standard polystyrene samples. The samples were analyzed by attenuated total reflection-Fourier-transform infrared (ATR-FTIR, FT/IR-4200, Jasco, Tokyo, Japan) spectroscopy. DLS measurements were performed at 25 °C using a Malvern (Malvern, UK) Zetasizer nano ZS at a scattering angle of 173°. The data were analyzed using a Malvern (Malvern, UK) Zetasizer Software package 7.11 to determine the hydrodynamic

radius (R_h), light scattering intensity (LSI), and polydispersity (PDI). SLS measurements were taken at 25 °C using an Otsuka Electronics (Osaka, Japan) DLS-7000. The weight-average molecular weight (M_w (SLS)) was calculated from Debye plots. The refractive index increment (dn/dc_p) was determined using an Otsuka Electronics (Osaka, Japan) DRM-3000 differential refractometer at 25 °C. Transmission electron microscopy (TEM, JEM-2100, Jeol, Tokyo, Japan) was performed at an acceleration voltage of 160 kV. The TEM samples were prepared by placing a drop of the sample solution on a copper grid coated with a form bar, and the samples were stained with a sodium phosphotungstate aqueous solution. The samples were dried for one day under reduced pressure. Fluorescence measurements were taken using a Hitachi High-Tech (Tokyo, Japan) F-2500 fluorescence spectrophotometer. The pyrene aqueous solutions (6.0×10^{-7} M) were excited at 334 nm; the excitation and emission slit widths were 20 and 2.5 nm, respectively.

3. Results and Discussion

3.1. Characterization

MEOM_{*n*} was prepared by SET-LRP using MEA and PEO-Br macroinitiator. The ¹H NMR spectra for PEO-Br and MEOM_{*n*} were measured in CDCl₃ (Figure 2). The terminal groups in PEO-Br could not be observed clearly because of the low signal intensity. The integral intensities of the PMEAs pendant methylene protons at 3.3 ppm (*e*) and the PEO main chain methylene protons at 3.5–4.0 ppm (*f*) were compared to estimate the DP (NMR = *n*) of one end of the PMEAs block in MEOM_{*n*}. The DP(NMR) values for MEOM₈₅ and MEOM₇₇₇ were 85 and 777, respectively (Table 1).

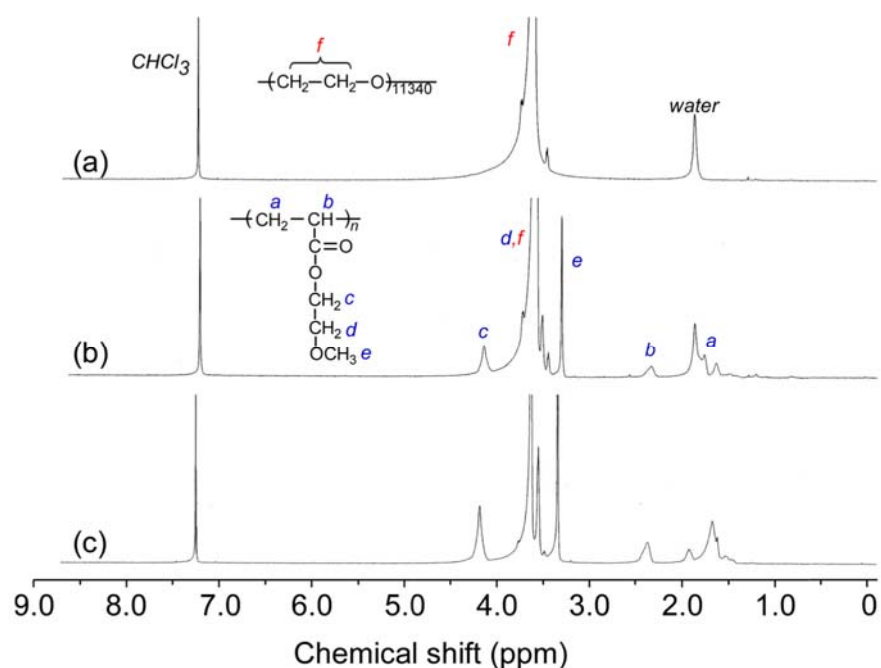


Figure 2. ¹H NMR spectra of (a) PEO-Br, (b) MEOM₈₅, and (c) MEOM₇₇₇ in CDCl₃.

Table 1. Characteristics of polymers.

Sample	$M_n(\text{Theo}) \times 10^5$	DP(Theo)	$M_n(\text{NMR}) \times 10^5$	DP(NMR)	$M_n(\text{GPC}) \times 10^5$	M_w/M_n (GPC)
PEO-Br	5.00 ^a	11,340 ^a	5.00	-	4.64	1.23
MEOM ₈₅	5.11	86 ^b	5.22	85 ^b	5.41	1.17
MEOM ₇₇₇	7.65	1020 ^b	7.02	777 ^b	4.91	1.26

^a These values of PEO base material were provided by the supplier. ^b Degree of polymerization of one end of PMEAs.

The theoretical DP(theo) and number average molecular weight ($M_n(\text{theo})$) can be calculated from the following equations:

$$\text{DP}(\text{theo}) = \frac{[M]_0}{[\text{Br}]_0} \times \frac{\text{Conversion} (\%)}{100} \quad (1)$$

$$M_n(\text{theo}) = \text{DP}(\text{theo}) \times M_n + M_{\text{PEO}} \quad (2)$$

where $[M]_0$ and $[\text{Br}]_0$ are the initial concentrations of the monomer and bromine atoms at the PEO-Br chain ends, respectively, and M_n and M_{PEO} are the molecular weights of the monomer and PEO, respectively. The DP(theo) values of MEOM₈₅ and MEOM₇₇₇ were 86 and 1020, respectively. These theoretical values were close to the DP(NMR) values. GPC was performed for MEOM_{*n*} using THF as an eluent (Figure S2). The structure of MEOM_{*n*} could be controlled because the M_w/M_n values estimated from GPC were less than 1.3. However, the retention time for the GPC elution curves of MEOM_{*n*} was similar to that of PEO-Br. Unexpected interactions may have occurred between the MEOM_{*n*} and GPC column, and polystyrene was used as the standard that may have impeded a correct estimation of the $M_n(\text{GPC})$ [29].

ATR-FTIR was performed to characterize the chemical structure of MEOM_{*n*} (Figure S3). The C=O vibration stretching peak was observed at 1700 cm⁻¹ for MEOM_{*n*}, whereas the peak could be observed for PEO-Br. The peak intensity at 1700 cm⁻¹ increased with increasing DP of the PMEAs block in MEOM_{*n*}. These results confirmed that MEOM_{*n*} had been prepared.

3.2. Association Behavior of MEOM_{*n*}

The R_h distributions of the flower micelles formed from MEOM_{*n*} in water were examined by DLS (Figure 3). MEOM₇₇₇ could not dissolve directly in water because of its long hydrophobic PMEAs blocks. Therefore, an aqueous solution was prepared to dialyze the THF solution of MEOM₇₇₇ against water. In contrast, MEOM₈₅ could dissolve directly in water. The R_h values of flower micelles obtained after directly dissolving them in water and after the dialysis method were compared to confirm the difference between the preparation methods of the MEOM₈₅ aqueous solutions (Figure S4). The R_h values for MEOM₈₅ prepared by direct dissolution in water and the dialysis method were 151 and 144 nm, respectively, which are similar. Therefore, flower micelles formed from MEOM₈₅ regardless of the solution preparation method. The association state of MEOM₈₅ that was easily soluble in water reaches the lowest association energy independently of the dissolution methods. Unless noted otherwise, the MEOM₈₅ aqueous solution was prepared using the direct dissolution method. The R_h distributions for MEOM_{*n*} in water were unimodal. The R_h values for MEOM₈₅ and MEOM₇₇₇ were 144 and 108 nm, respectively. The DP of the hydrophobic PMEAs block in MEOM₇₇₇ was larger than that in MEOM₈₅, but R_h of MEOM₇₇₇ was smaller than that of MEOM₈₅. As the DP of the PMEAs block in MEOM_{*n*} increased, the hydrophobic interaction became stronger to form a more compact core of the flower micelle. The PDI values for MEOM₈₅ and MEOM₇₇₇ were 0.166 and 0.211, respectively. MEOM₈₅ formed more uniformly sized flower micelles than MEOM₇₇₇.

The structure of flower micelles formed from MEOM_{*n*} in water was confirmed by SLS (Figure S5). The apparent weight-average molecular weight ($M_w(\text{SLS})$) and radius of gyration (R_g) were obtained from the SLS measurements. The refractive index increment (dn/dc_p) required to determine $M_w(\text{SLS})$ was obtained using a differential refractometer. The dn/dc_p values for MEOM₈₅ and MEOM₇₇₇ were 0.138 and 0.426 mL/g, respectively. The number of PMEAs chains (N_{agg}) forming a single flower micelle was calculated from the equation, $N_{\text{agg}} = 2M_w(\text{SLS}) / (M_n(\text{NMR}) \times M_w/M_n)$. The N_{agg} values for MEOM₈₅ and MEOM₇₇₇ were 156 and 164, respectively (Table 2). The DP of the PMEAs block in MEOM₇₇₇ was approximately nine times larger than that in MEOM₈₅, but both N_{agg} values were close. The interface between the core and shell was sterically crowded with the PEO chains because the DP of the PEO block forms a loop-shaped shell. It was unlikely that the N_{agg}

value would increase above a certain number because of the congestion of the PEO shell chains on the core–shell interface. The R_g values for MEOM₈₅ and MEOM₇₇₇ were 141 and 164 nm, respectively. From the R_h and R_g values, the flower micelles formed from MEOM₈₅ and MEOM₇₇₇ have similar size. The R_g/R_h ratios for MEOM₈₅ and MEOM₇₇₇ were 0.934 and 1.52, respectively. These R_g/R_h ratios were close to one, suggesting that the shape of flower micelles was spherical [30]. The density (Φ_H) of the micelle can be calculated from Equation (3) [31]:

$$\Phi_H = \frac{M_w(\text{SLS})}{N_A} \left(\frac{4}{3} \pi R_h^3 \right)^{-1} \quad (3)$$

where N_A is Avogadro's number. The Φ_H values for MEOM₈₅ and MEOM₇₇₇ were 5.47×10^{-3} and 2.29×10^{-2} g/mL, respectively. MEOM₇₇₇ with a long PMEA chain formed a tightly packed core because the Φ_H value of MEOM₇₇₇ was larger than that of MEOM₈₅; ^1H NMR spectroscopy of MEOM_{*n*} was performed in D₂O (Figure S6). The PEO signals were observed, but the PMEA signals were not. This observation suggests that the motion of PMEA was restricted due to the formation of the core, but the motion of PEO was not restricted.

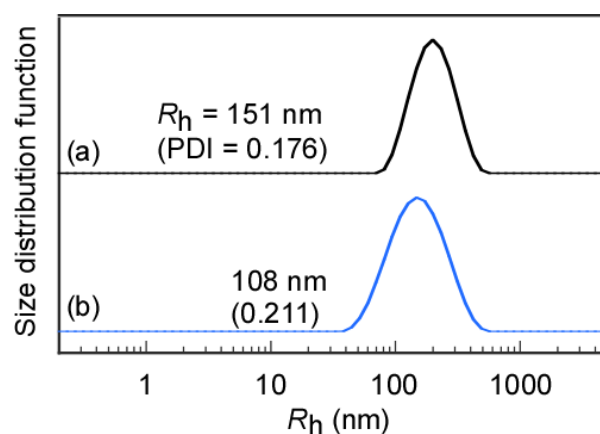


Figure 3. Hydrodynamic radius (R_h) distributions of (a) MEOM₈₅ and (b) MEOM₇₇₇ in water at $C_p = 0.1$ g/L.

Table 2. Characteristics of MEOM_{*n*} flower-like micelles in water.

Sample	$M_w(\text{SLS})^a \times 10^{-7}$ (g/mol)	R_g^a (nm)	R_h^b (nm)	R_g/R_h	R_{TEM}^c (nm)	$N_{\text{agg}}(\text{SLS})^d$	$\Phi_H \times 10^2$ (g/mL)
MEOM ₈₅	4.75	141	151	0.934	42.4	156	0.547
MEOM ₇₇₇	7.27	164	108	1.52	59.2	164	2.29

^a Estimated from SLS measurements; ^b estimated from DLS measurements; ^c estimated from TEM; ^d calculated from $2M_w(\text{SLS})/(M_n(\text{NMR}) \times M_w/M_n)$.

TEM of MEOM₈₅ and MEOM₇₇₇ in water (Figure 4) revealed spherical aggregates. The radii (R_{TEM}) of MEOM₈₅ and MEOM₇₇₇ estimated from TEM were 42.4 and 59.2 nm, respectively. These R_{TEM} values were smaller than R_h and R_g obtained from light scattering measurements. The shells formed from PEO were not observed because PEO cannot be stained by sodium phosphotungstate. The core formed by the association of the PMEA blocks could be stained, as observed by TEM. Therefore, the cores observed by TEM were separated a certain distance due to the unstained PEO loop shells that cannot be observed by TEM.

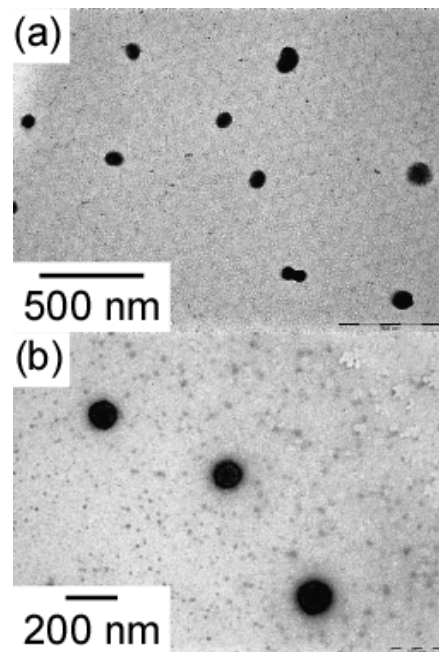


Figure 4. TEM images for (a) MEOM₈₅ and (b) MEOM₇₇₇ in water at $C_p = 0.1$ g/L.

3.3. Critical Micelle Concentration (CMC) of MEOM_n

To determine the CMC of flower micelles, the LSI for MEOM_n aqueous solutions was measured as a function of C_p (Figure 5). The ratio (I/I_0) of the LSI of the solution (I) to the solvent (I_0) was plotted as a function of C_p . The CMC was estimated from the inflection point of the slope [32]. The CMC values for MEOM₈₅ and MEOM₇₇₇ were calculated to be 0.01 and 0.002 g/L, respectively (Table 3).

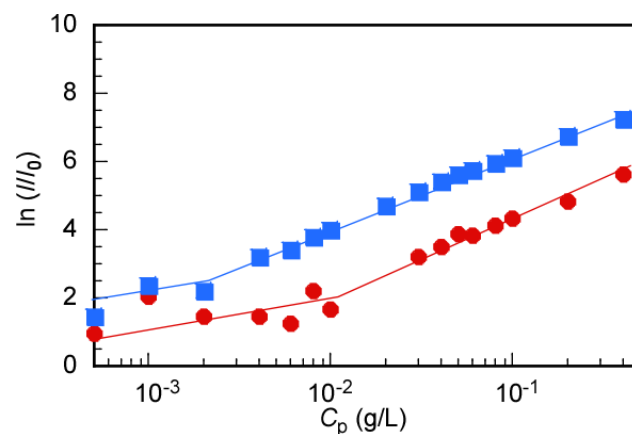


Figure 5. Light scattering intensity (LSI) ratio (I/I_0) as a function of polymer concentration (C_p) for MEOM₈₅ (●) and MEOM₇₇₇ (■) in aqueous solutions; I_0 is LSI of water, and I is LSI of the polymer solution.

Table 3. Critical micelle concentration (CMC) of MEOM_n.

Sample	CMC(LSI) (g/L)	CMC(Em) (g/L)	CMC(Ex) (g/L)
MEOM ₈₅	0.01	0.01	0.01
MEOM ₇₇₇	0.002	0.0015	0.002

The CMC of MEOM_{*n*} was also estimated using pyrene as a hydrophobic fluorescence probe (Figure 6). The intensity ratio (I_3/I_1) of the first (I_1) to third vibronic peak (I_3) of the pyrene fluorescence spectrum depends on the microenvironmental polarity around the pyrene molecule [33]. I_3/I_1 increased with decreasing microenvironmental polarity. I_3/I_1 was plotted as a function of C_p to determine the CMC (CMC(Em)) (Figure 6). CMC(Em) was calculated from the intersections of the two tangents of the plots. The CMC(Em) values for MEOM₈₅ and MEOM₇₇₇ were 0.01 and 0.0015 g/L, respectively. The emission maximum wavelength of the 0–0 band in the pyrene excitation spectrum shifts to a longer wavelength when the microenvironment around the pyrene molecule becomes hydrophobic [34]. The 0–0 band maximum wavelengths of the aqueous solutions in the presence and absence of MEOM_{*n*} were 338 and 335 nm, respectively. The CMC (CMC(Ex)) was determined from a plot of I_{338}/I_{335} vs. C_p , where I_{338} and I_{335} are the emission intensities at 338 and 335 nm, respectively. The CMC(Ex) values for MEOM₈₅ and MEOM₇₇₇ were 0.01 and 0.002 g/L, respectively. The CMC values estimated from the LSI and fluorescence probe methods were similar. These observations suggest that hydrophobic anticancer drugs can be encapsulated in the core above the CMC.

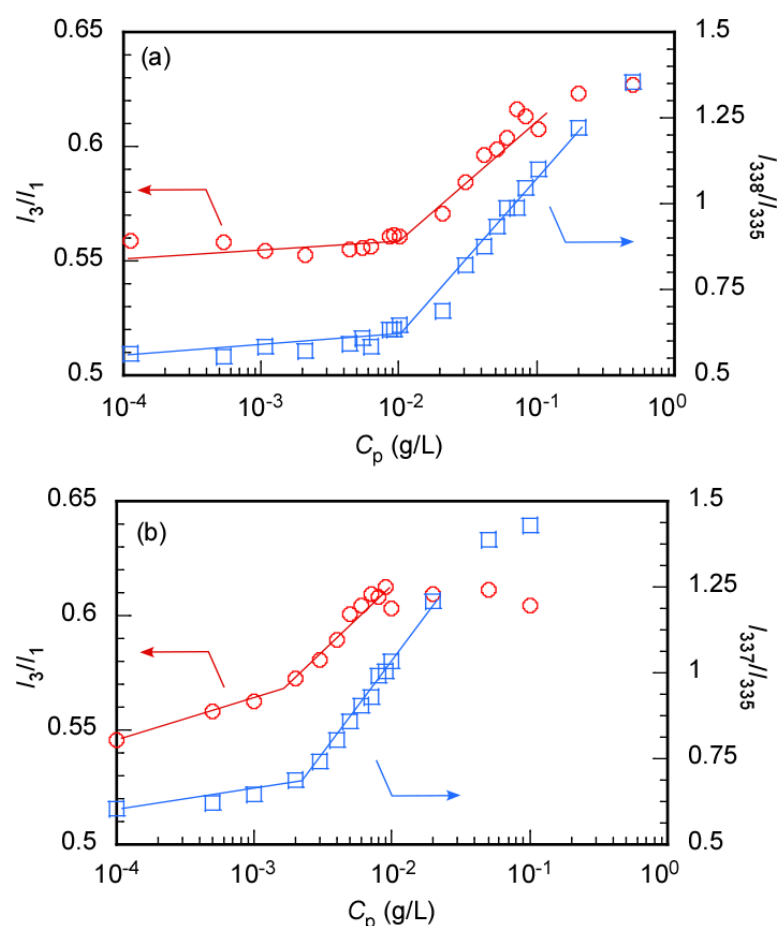


Figure 6. Pyrene fluorescence intensity ratio (I_3/I_1 , \circ) and excitation intensity ratio (I_{338}/I_{335} , \square) as a function of the polymer concentration (C_p) for (a) MEOM₈₅ and (b) MEOM₇₇₇ in aqueous solutions; I_3 and I_1 are the third and first vibronic peak intensities of pyrene fluorescence, and I_{338} and I_{335} are the peak intensities at 338 and 335 nm in the excitation spectra of pyrene.

4. Conclusions

Amphiphilic ABA triblock copolymers, MEOM_{*n*}, were prepared via SET-LRP using a bifunctional PEO-Br macroinitiator. MEOM₈₅ and MEOM₇₇₇ were prepared with different DP of the hydrophobic PMEAs at the central PEO chain ends. The DP of the PMEA block in MEOM₇₇₇ was approximately nine times larger than that of MEOM₈₅. The R_h values for flower micelles formed from MEOM₈₅ and MEOM₇₇₇ in water were 151 and 108 nm, respectively. The hydrophobic PMEA blocks with a large DP in MEOM₇₇₇ associated to form a densely packed core due to the strong hydrophobic interactions. The N_{agg} values for flower micelles formed from MEOM₈₅ and MEOM₇₇₇ were similar. The CMC for MEOM₈₅ and MEOM₇₇₇ were 0.01 and 0.002 g/L, respectively. The CMC of MEOM₇₇₇ was smaller than that of MEOM₈₅ because of the strong hydrophobic interactions of MEOM₇₇₇. These results may come from much larger DP of the PEO block than that of the PMEA blocks. The PEO blocks that formed the loop shells of flower micelles and the PMEA blocks that formed the core were both biocompatible. Therefore, the biocompatible flower micelles formed from MEOM_{*n*} may have applications as novel drug delivery carriers. We believe that the chemical design of MEOM_{*n*} can be applied for coating on the various biomedical devices.

Supplementary Materials: The following are available online at <https://www.mdpi.com/article/10.3390/polym14091678/s1>, Scheme S1. Synthesis of MEOM_{*n*} ($n = 85$ and 777); Figure S1. Mechanism of single-electron transfer-living radical polymerization (SET-LRP); M; monomer, P; polymer, Cu; copper, X; halogen, L; ligand, kact; activation, kdeact; deactivation, kp; propagation, kt; termination; Figure S2. Gel-permeation chromatography (GPC) elution curves of PEO11340-Br (black line), MEOM₈₅ (red line), and MEOM₇₇₇ (blue line) using THF as an eluent with a flow rate of 1.0 mL/min at 40 °C; Figure S3. Attenuated total reflection (ATR) Fourier-transform infrared (FTIR) spectra for (a) PEO11340-Br, (b) MEOM₈₅, and (c) MEOM₇₇₇; Figure S4. Hydrodynamic radius (R_h) distributions of MEOM₈₅ aqueous solution prepared by directly dissolution (blue line) and by dialysis from THF solution against aqueous solution (red line); the final polymer concentration (C_p) was adjusted to 0.1 g/L; Figure S5. Debye plots for (a) MEOM₈₅ and (b) MEOM₇₇₇ in water; Figure S6. Water suppression by gradient-tailored excitation (WATERGATE) ¹H NMR spectroscopy in D₂O for (a) MEOM₈₅ and (b) MEOM₇₇₇ at 25 °C.

Author Contributions: Conceptualization and experimental design: K.H. and S.-i.Y.; Experimental work and data analysis: Y.M. and E.O.; writing: Y.M., K.H. and S.-i.Y. All authors have read and agreed to the published version of the manuscript.

Funding: This research was partially supported by KAKENHI grants (21H02005, 21K19931, 21H05027, 21H05535) from the Japan Society for the Promotion of Science (JSPS), JSPS Bilateral Joint Research Projects (JPJSBP120203509), the Cooperative Research Program of “Network Joint Research Center for Materials and Devices (20214044)”, the International Collaborative Research Program of Institute for Chemical Research, Kyoto University (2022–121), and MEXT Promotion of Distinctive Joint Research Center Program (JPMXP 0621467946).

Institutional Review Board Statement: Not applicable.

Informed Consent Statement: Not applicable.

Data Availability Statement: Not applicable.

Conflicts of Interest: The authors declare no conflict of interest.

References

1. Shi, Y.; Van Nostrum, C.F.; Hennink, W.E. Interfacially hydrazone cross-linked thermosensitive polymeric micelles for acid-triggered release of paclitaxel. *ACS Biomater. Sci. Eng.* **2015**, *1*, 393–404. [[CrossRef](#)] [[PubMed](#)]
2. Honda, S.; Yamamoto, T.; Tezuka, Y. Topology-directed control on thermal stability: Micelles formed from linear and cyclized amphiphilic block copolymers. *J. Am. Chem. Soc.* **2010**, *132*, 10251–10253. [[CrossRef](#)] [[PubMed](#)]
3. Yuan, F.; Larson, R.G. Multiscale molecular dynamics simulations of model hydrophobically modified ethylene oxide urethane micelles. *J. Phys. Chem. B* **2015**, *119*, 12540–12551. [[CrossRef](#)] [[PubMed](#)]
4. Lundberg, D.J.; Brown, R.G.; Glass, J.E.; Eley, R.R. Synthesis, characterization, and solution rheology of model hydrophobically-modified, water-soluble ethoxylated urethanes. *Langmuir* **1994**, *10*, 3027–3034. [[CrossRef](#)]

5. Maiti, S.; Chatterji, P.R. Transition from normal to flower like micelles. *J. Phys. Chem. B* **2000**, *104*, 10253–10257. [[CrossRef](#)]
6. Vorobyova, O.; Yekta, A.; Winnik, M.A.; Lau, W. Fluorescent probe studies of the association in an aqueous solution of a hydrophobically modified poly(ethylene oxide). *Macromolecules* **1998**, *31*, 8998–9007. [[CrossRef](#)]
7. Gref, R.; Lück, M.; Quellec, P.; Marchand, M.; Dellacherie, E.; Harnisch, S.; Blunk, T.; Müller, R.H. “Stealth” corona-core nanoparticles surface modified by polyethylene glycol (PEG): Influences of the corona (PEG chain length and surface density) and of the core composition on phagocytic uptake and plasma protein adsorption. *Colloids Surf. B Biointerfaces* **2000**, *18*, 301–313. [[CrossRef](#)]
8. De Graaf, A.J.; Boere, K.W.M.; Kemmink, J.; Fokkink, R.G.; Van Nostrum, C.F.; Rijkers, D.T.S.; Van Der Gucht, J.; Wienk, H.; Baldus, M.; Mastrobattista, E.; et al. Looped structure of flower like micelles revealed by ¹H NMR relaxometry and light scattering. *Langmuir* **2011**, *27*, 9843–9848. [[CrossRef](#)]
9. Kelarakis, A.; Yang, Z.; Pousia, E.; Nixon, S.K.; Price, C.; Booth, C.; Hamley, I.W.; Castelletto, V.; Fundin, J. Association properties of diblock copolymers of propylene oxide and ethylene oxide in aqueous solution. The effect of P and E block lengths. *Langmuir* **2001**, *17*, 8085–8091. [[CrossRef](#)]
10. Riess, G. Micellization of block copolymers. *Prog. Polym. Sci.* **2003**, *28*, 1107–1170. [[CrossRef](#)]
11. Atanase, L.I.; Riess, G. Self-Assembly of Block and Graft Copolymers in Organic Solvents: An Overview of Recent Advances. *Polymers* **2018**, *10*, 62. [[CrossRef](#)] [[PubMed](#)]
12. Zhulina, E.B.; Adam, M.; LaRue, I.; Sheiko, S.S.; Rubinstein, M. Diblock Copolymer Micelles in a Dilute Solution. *Macromolecules* **2005**, *38*, 5330–5351. [[CrossRef](#)]
13. Wang, C.H.; Hsiue, G.H. New amphiphilic poly(2-ethyl-2-oxazoline)/poly(L-lactide) triblock copolymers. *Biomacromolecules* **2003**, *4*, 1487–1490. [[CrossRef](#)] [[PubMed](#)]
14. Borisov, O.V.; Halperin, A. Micelles of polysoaps. *Langmuir* **1995**, *11*, 2911–2919. [[CrossRef](#)]
15. Zhang, N.; Samanta, S.R.; Rosen, B.M.; Percec, V. Single electron transfer in radical ion and radical-mediated organic, materials and polymer synthesis. *Chem. Rev.* **2014**, *114*, 5848–5958. [[CrossRef](#)]
16. Lligadas, G.; Grama, S.; Percec, V. Single-electron transfer living radical polymerization platform to practice, develop, and invent. *Biomacromolecules* **2017**, *18*, 2981–3008. [[CrossRef](#)]
17. Najafi, M.; Kordalivand, N.; Moradi, M.A.; Van Den Dikkenberg, J.; Fokkink, R.; Friedrich, H.; Sommerdijk, N.A.J.M.; Hembury, M.; Vermonden, T. Native chemical ligation for cross-linking of flower-like micelles. *Biomacromolecules* **2018**, *19*, 3766–3775. [[CrossRef](#)]
18. Oh, K.T.; Oh, Y.T.; Oh, N.M.; Kim, K.; Lee, D.H.; Lee, E.S. A smart flower-like polymeric micelle for pH-triggered anticancer drug release. *Int. J. Pharm.* **2009**, *375*, 163–169. [[CrossRef](#)]
19. Baek, A.; Baek, Y.M.; Kim, H.M.; Jun, B.H.; Kim, D.E. Polyethylene glycol-grafted graphene oxide as biocompatible materials for peptide nucleic acid delivery into cells. *Bioconjug. Chem.* **2018**, *29*, 528–537. [[CrossRef](#)]
20. Tanaka, M.; Motomura, T.; Kawada, M.; Anzai, T.; Kasori, Y.; Shiroya, T.; Shimura, K.; Onishi, M.; Mochizuki, A. Blood compatible aspects of poly(2-methoxyethylacrylate) (PMEA)-relationship between protein adsorption and platelet adhesion on PMEA surface. *Biomaterials* **2000**, *21*, 1471–1481. [[CrossRef](#)]
21. Steinhauer, W.; Hoogenboom, R.; Keul, H.; Moeller, M. Copolymerization of 2-hydroxyethyl acrylate and 2-methoxyethyl acrylate via RAFT: Kinetics and thermoresponsive properties. *Macromolecules* **2010**, *43*, 7041–7047. [[CrossRef](#)]
22. Tanaka, M.; Mochizuki, A.; Ishii, N.; Motomura, T.; Hatakeyama, T. Study of blood compatibility with poly(2-methoxyethyl acrylate). Relationship between water structure and platelet compatibility in poly(2-methoxyethylacrylate-co-2-hydroxyethylmethacrylate). *Biomacromolecules* **2002**, *3*, 36–41. [[CrossRef](#)] [[PubMed](#)]
23. Liu, G.; Qiu, Q.; Shen, W.; An, Z. Aqueous dispersion polymerization of 2-methoxyethyl acrylate for the synthesis of biocompatible nanoparticles using a hydrophilic RAFT polymer and a redox initiator. *Macromolecules* **2011**, *44*, 5237–5245. [[CrossRef](#)]
24. Liu, G.; Jin, Q.; Liu, X.; Lv, L.; Chen, C.; Ji, J. Biocompatible vesicles based on PEO-*b*-PMPC/ α -cyclodextrin inclusion complexes for drug delivery. *Soft Matter* **2011**, *7*, 662–669. [[CrossRef](#)]
25. Mueller, X.M.; Jegger, D.; Augstburger, M.; Horisberger, J.; Von Segesser, L.K. Poly2-methoxyethylacrylate (PMEA) coated oxygenator: An ex vivo study. *Int. J. Artif. Organs* **2002**, *25*, 223–229. [[CrossRef](#)]
26. Haraguchi, K.; Kubota, K.; Takada, T.; Mahara, S. Highly protein-resistant coatings and suspension cell culture thereon from amphiphilic block copolymers Prepared by RAFT polymerization. *Biomacromolecules* **2014**, *15*, 1992–2003. [[CrossRef](#)]
27. Haraguchi, K.; Takehisa, T.; Mizuno, T.; Kubota, K. Antithrombogenic properties of amphiphilic block copolymer coatings: Evaluation of hemocompatibility using whole blood. *ACS Biomater. Sci. Eng.* **2015**, *1*, 352–362. [[CrossRef](#)]
28. Filippov, S.K.; Bogomolova, A.; Kabarov, L.; Velychkivska, N.; Starovoytova, L.; Cernochova, Z.; Rogers, S.E.; Lau, W.M.; Khutoryanskiy, V.V.; Cook, M.T. Internal nanoparticle structure of temperature-responsive self-assembled PNIPAM-*b*-PEG-*b*-PNIPAM triblock copolymers in aqueous solutions: NMR, SANS, and light scattering studies. *Langmuir* **2016**, *32*, 5314–5323. [[CrossRef](#)]
29. Meier, M.A.R.; Lohmeijer, B.G.G.; Schubert, U.S. Characterization of defined metal-containing supramolecular block copolymers. *Macromol. Rapid Commun.* **2003**, *24*, 852–857. [[CrossRef](#)]
30. Akcasu, A.Z.; Han, C.C. Molecular weight and temperature dependence of polymer dimensions in solution. *Macromolecules* **1979**, *12*, 276–280. [[CrossRef](#)]

31. Tahara, Y.; Sakiyama, M.; Takeda, S.; Nishimura, T.; Mukai, S.A.; Sawada, S.I.; Sasaki, Y.; Akiyoshi, K. Self-assembled nanogels of cholesterol-bearing hydroxypropyl cellulose: A thermoresponsive building block for nanogel tectonic materials. *Langmuir* **2016**, *32*, 12283–12289. [[CrossRef](#)] [[PubMed](#)]
32. Topel, Ö.; Çakir, B.A.; Budama, L.; Hoda, N. Determination of critical micelle concentration of polybutadiene-*block*-poly(ethyleneoxide) diblock copolymer by fluorescence spectroscopy and dynamic light scattering. *J. Mol. Liq.* **2013**, *177*, 40–43. [[CrossRef](#)]
33. Kalyanasundaram, K.; Thomas, J.K. Environmental effects on vibronic and intensities in pyrene monomer fluorescence and their application in studies of micellar systems. *J. Am. Chem. Soc.* **1977**, *99*, 2039–2044. [[CrossRef](#)]
34. Xu, J.P.; Ji, J.; Chen, W.D.; Shen, J.C. Novel biomimetic surfactant: Synthesis and micellar characteristics. *Macromol. Biosci.* **2005**, *5*, 164–171. [[CrossRef](#)]